International Journal of Refrigeration 157 (2024) 73–85

Contents lists available at ScienceDirect

International Journal of Refrigeration

journal homepage: www.elsevier.com/locate/ijrefrig

A novel spherical micro-absorber for dehumidification systems

Un nouveau micro-absorbeur sphérique pour les systèmes de déshumidification

Amin M. Elsafi, Majid Bahrami *

Laboratory for Alternative Energy Conversion (LAEC), School of Mechatronic Systems Engineering, Simon Fraser University, Surrey, BC, V3T 0A3, Canada

ARTICLE INFO

Keywords:
Liquid desiccant
Dehumidification
Microfluidics
Membrane
Absorption systems
Mots clés:
Déshydratant liquid
Déshumidification
Microfluidique
Membrane
Systèmes à absorption

ABSTRACT

In this work, a novel design concept for absorbers used in dehumidification systems is proposed to overcome the practical challenges of the conventional packed-column absorbers. In the proposed design, spherical micro-absorbers (microcapsules) that contain a liquid LiBr desiccant inside a semi-permeable polymeric membrane shell are produced by using a custom-built microfluidic technique. The produced microcapsules are capable of containing the salt during crystallization. The X-ray diffraction analysis has confirmed that the observed crystals in the microscopes images were indeed for the encapsulated (LiBr) salt. Due to the indirect contact between the liquid desiccant and the process air, problems such as solution carryover and corrosion associated with packed-column absorbers can be eliminated. The collected sorption data show that the spherical microcapsules offer a high sorption capacity of 1 g_w/g_{dry} under 80% relative humidity. The proposed microcapsules offer surface-to-volume ratios between 6,000–12,000 m^2/m^3, which is up to two orders of magnitude higher than the conventional packed-column absorbers (200–600 m^2/m^3). The produced micro-absorbers can withstand a compression force up to 2×10^5 their weight, elastically expanded during the absorption process without rupture, and did not show a leakage or a reduction in capacity even after an accelerated test of 200 sorption-desorption cycles.

1. Introduction

The required energy to control the temperature and humidity for human comfort is estimated as 50% of the building's total energy consumption (Rafique et al., 2016). Several serious health problems which are caused by mildew, viruses, and reduction of air quality in buildings are all associated with excessive humidity (Guieysse et al., 2008). Humidity control also plays a vital role in greenhouse food production. Low humidity leads to reduced stem lengths and leaf sizes, while excessive humidity along with condensation can lead to fungal diseases, leaf necrosis, and soft and thin leaves (Farooq et al., 2009).

Air dehumidification can be achieved using heat pumps (cooling-condensation), membrane-based heat/enthalpy exchangers, and sorption (solid or liquid desiccant) desiccant dehumidification systems among other technologies. Despite their high efficiency, using heat pumps for dehumidification comes with challenges, such as high initial and operating costs, maintenance issues, ozone depletion potential, and global warming potential. On the other hand, membrane-based heat/enthalpy exchangers are simple, inexpensive, and have an overall efficiency of 60–90% (Nizovtsev et al., 2016; Fernández-Seara et al., 2011), but they are prone to frost formation in cold climates and are less effective during the summer periods (Han et al., 2015). Utilizing thermally driven sorption systems helps to alleviate the burden on the electricity generation sector, and can significantly reduce the emissions associated with ventilation and air conditioning systems, particularly, when waste-heat or renewable energy source are used. Waste-heat (sources with temperature <100 °C) is abundant energy that can be harvested from various sources, such as industrial facilities, data centers, fuel cells, and solar thermal panels, to name a few. Typical solid desiccant dehumidifiers use zeolite as an adsorbent material because it has a higher sorption capacity than silica gel. These systems require a relatively high regeneration temperature in the range of 90–260 °C (Mei et al., 1992; Singh et al., 2018; Qi et al., 2020). On the other hand, liquid desiccant hygroscopic salt absorbents, such as LiBr, LiCl, and $CaCl_2$ have a higher sorption capacity than solid adsorbents and a low regeneration temperature (60–90 °C) (Dong et al., 2019).

Nevertheless, the research on liquid desiccant dehumidification systems (using hygroscopic salts) is limited to laboratory-scale experiments rather than practical applications in buildings (Qi et al., 2020). A packed-column absorber that operates in the falling-film mode is the most popular design used in liquid desiccant dehumidifiers due to its

* Corresponding author.
E-mail addresses: amin_elsafi@yahoo.com (A.M. Elsafi), mbahrami@sfu.ca (M. Bahrami).

https://doi.org/10.1016/j.ijrefrig.2023.11.006
Received 21 July 2023; Received in revised form 28 October 2023; Accepted 5 November 2023
Available online 10 November 2023

Nomenclature

Abbreviation

CV	coefficient of variation
I.D.	inner diameter
O.D.	outer diameter
TGA	thermogravimetric analyzer
TMA	thermomechanical analyzer
W/O/W	water-in oil-in water
O/W/O	oil- in water-in oil

Roman Symbols

D	diameter, m
P	pressure, kPa
Q	flow rate, mL/h
RH	relative humidity, -
t	thickness, m
T	temperature, °C

Subscripts

i	shell's inner diameter
I	inner fluid
M	middle fluid
o	shell's outer diameter
O	outer (carrier) fluid
shell	capsules' shell

high effectiveness and low pressure drop (Elsarrag et al., 2005). The main mechanism for the mass transfer in such packed-column absorbers is the diffusion through the liquid solution film, which is a rather slow process and presents a fundamental limitation on the maximum performance that can be achieved. In such absorbers, the humid air is brought into direct contact with a concentrated salt solution to absorb the moisture. However, there is a high risk of solution carryover into the airstream. Inhaling air contaminated with salt particles can cause problems in the human respiratory system. Problems such as salt crystallization and corrosion should also be addressed for practical applications (Qi et al., 2020; Chugh et al., 2017; Jain and Bansal, 2007). Corrosion due to the salt-metal contact significantly reduces the lifetime of the absorber and the dehumidification system. Crystallization should also be avoided in liquid flowing systems because it leads to the formation of solids that can block the piping network and cause damage to the pumping system. Dissolving the crystallized salt to restore the absorber operation is a labor intensive and time consuming process (Liao and Radermacher, 2007; Wang et al., 2011). Developing an absorber that can work in the crystallization region allows a significant increase in the working capacity.

Studies have shown that membrane-based absorbers can enhance the absorption rates due to the thin solution (film) thickness and reduce heat and mass transfer resistance compared to the falling-film absorbers (Ali and Schwerdt, 2009). However, there are some challenges that should be overcome for their practical use. Membranes are usually prone to fouling and the risk for pore blocking increases with the use of salt solutions that can crystallize. Another reason that can result in the blocking of the pores is the condensation of water vapor. As the membrane thickness in these absorbers was thin (~100 μm), the design process should ensure that the mechanical strength requirements were fulfilled.

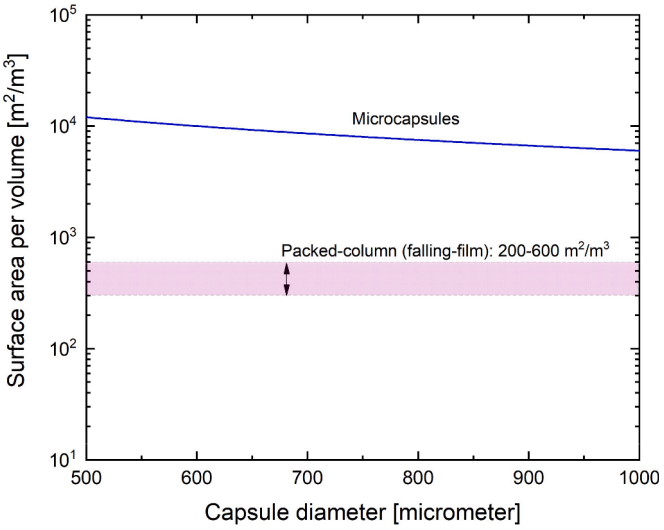

Fig. 2. The reaction surface area per volume for microcapsules and packed-column absorber (Bhowmik et al., 2021; Liu et al., 2011; Chen et al., 2017; Tan et al., 2012; Longo and Gasparella, 2006; Bassuoni, 2011).

In this work, a novel design concept for absorbers is proposed that can be used for dehumidification systems. The proposed absorber provides compactness (i.e., high surface area per volume), permits working in the crystallization region, and eliminates the metal corrosion associated with the corrosive hygroscopic salts. This is achieved by creating spherical micro-absorbers by encapsulating an aqueous hygroscopic salt (e.g., LiBr, LiCl, or $CaCl_2$) solution inside an elastic semi-permeable

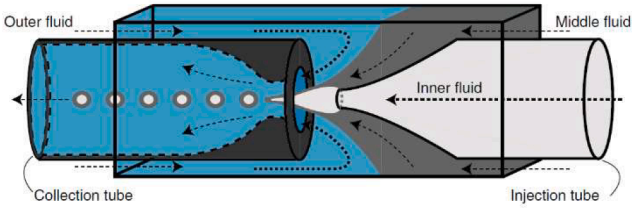

Fig. 3. Illustration of the glass-capillary microfluidic device invented by Utada et al. (Utada et al., 2007) for double-emulsion formation.

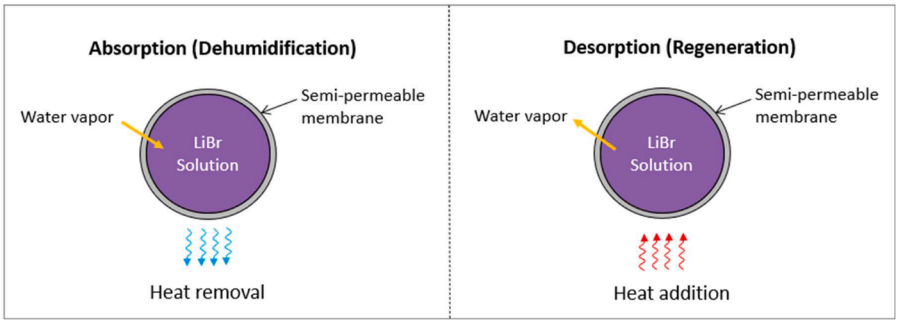

Fig. 1. Absorption and regeneration principles of the proposed spherical microreactor for dehumidification applications.

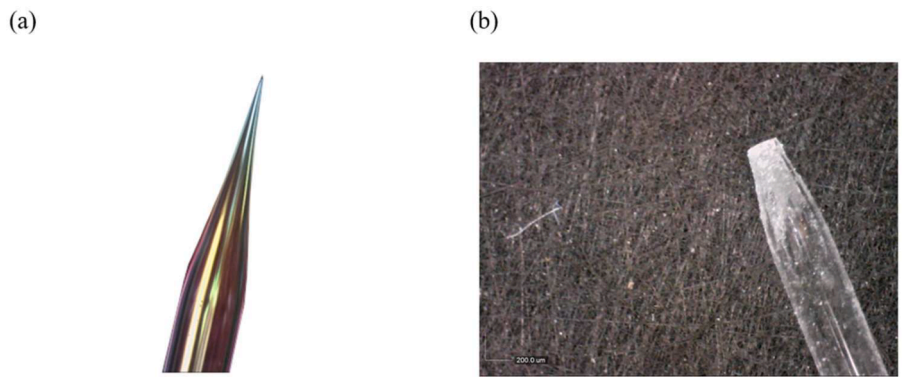

Fig. 4. (a) Injection and (b) collection glass capillary tubes.

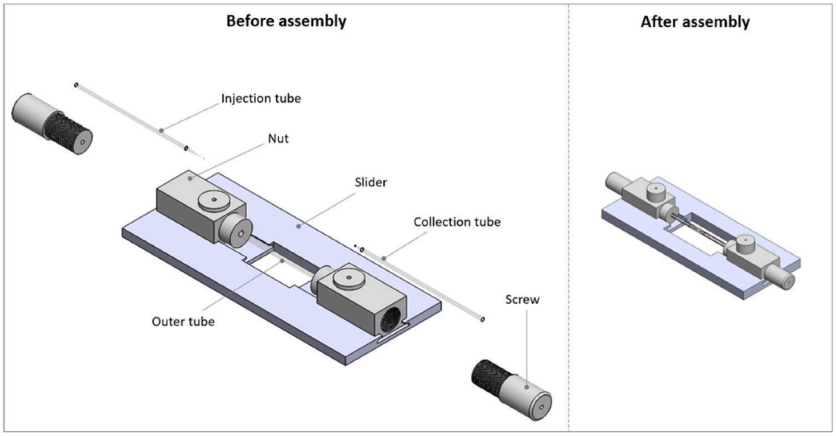

Fig. 5. A 3D CAD drawing of the microfluidic device before and after assembly.

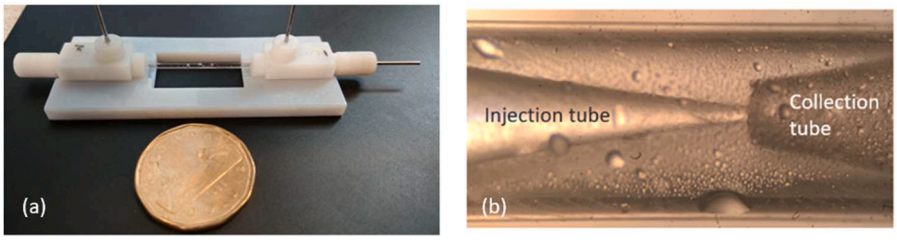

Fig. 6. (a) An assembled 3D printed microfluidic device; besides a Canadian 1-dollar coin for size reference; and (b) the alignment of the glass capillary tubes.

membrane shell. The shell is highly permeable to sorbate but impermeable to the salt and its solution. Due to the indirect contact between the liquid desiccant and the air, problems such as solution carryover and corrosion can be completely eliminated. A study on carbon dioxide (CO_2) capture using a similar encapsulation technique with an elastic shell has shown that the absorption rates for the encapsulated carbonate solutions were 10 folds higher than in a 1 mm thick film of a carbonate solution that usually forms in the conventional packed-column absorbers (Vericella et al., 2015).

The working principles of the spherical microreactors during absorption (dehumidification) and regeneration processes is illustrated in Fig. 1. The sorbate (water vapor) diffuses through the shell and is absorbed by the absorbent (salt solution) in the absorption process. In the desorption process, heat is transferred to the capsule to desorb the water vapor to increase the salt concentration for the next absorption cycle.

The formed spherical micro-absorbers (i.e., microcapsules) are highly uniform in size and can be designed to have a micro-scale size (500–1000 μm diameter) and have an adjustable shell thickness. They provide a high reaction surface-to-volume ratio that allows fast absorption rates, therefore, more compact absorber designs. As shown in Fig. 2, the proposed microcapsules offer surface-to-volume ratios

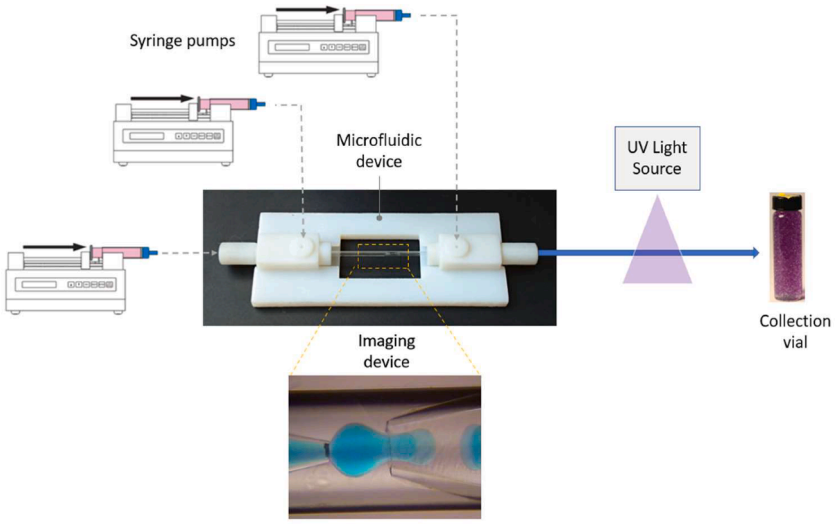

Fig. 7. A schematic of the microfluidic experimental setup.

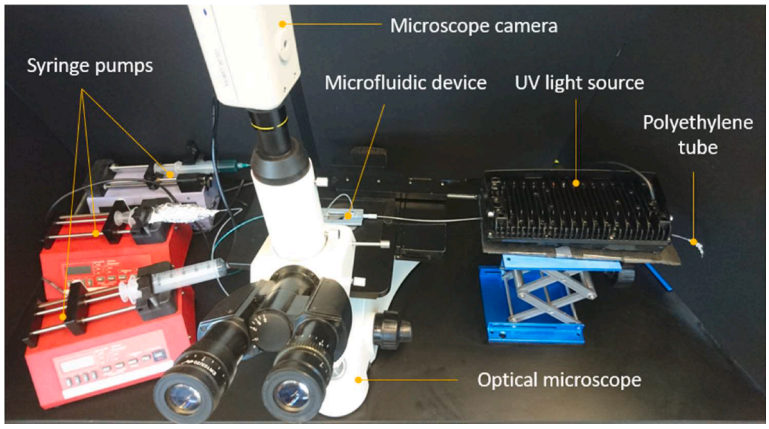

Fig. 8. The microfluidic experimental setup.

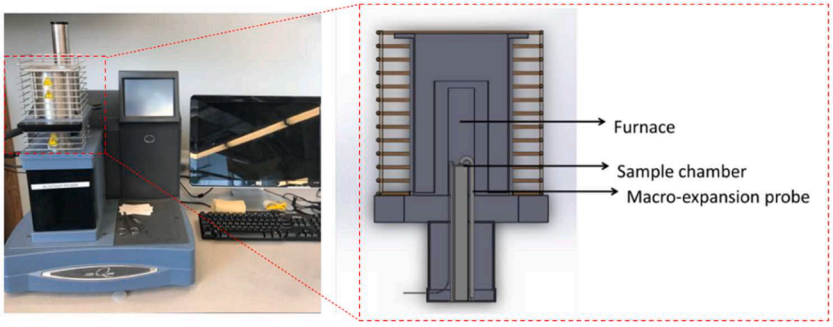

Fig. 9. The thermomechanical analyzer (Q400EM, TA instruments).

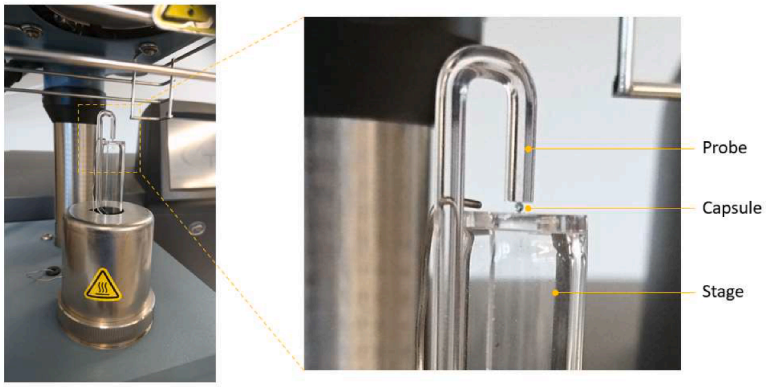

Fig. 10. Microcapsules under compression testing.

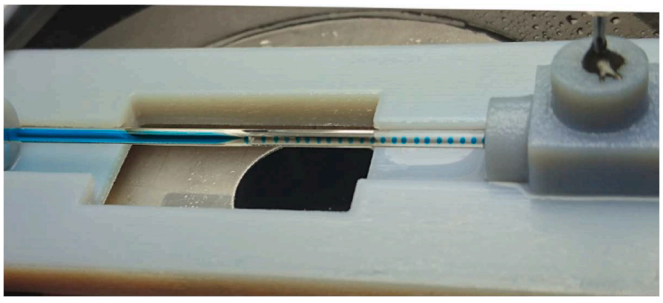

Fig. 11. The custom-built microfluidic device under operation.

(defined as the ratio between the surface area to the volume of a "single" sphere) between 6000 and 12,000 m^2/m^3, which is up to two orders of magnitude higher than the conventional packed-column absorbers (200–600 m^2/m^3 (Bhowmik et al., 2021; Liu et al., 2011; Chen et al., 2017; Tan et al., 2012; Longo and Gasparella, 2006; Bassuoni, 2011)).

2. Materials and methods

2.1. Encapsulation of liquid desiccants using microfluidic technique

In the present study, a microfluidic technique described by Utada et al. (Utada et al., 2005) was used as a platform to create a water-in-oil-in-water (W/O/W) double emulsion in order to encapsulate the aqueous liquid sorbent solutions (water-phase) inside a polymeric shell material (oil-phase). An illustration of the microfluidic device working principle is shown in Fig. 3. Two rounded glass capillary tubes are laid end to end within an outer square or circular glass tube. The inner fluid is pumped from the tapered end of the glass injection tube to the larger tip of the round capillary (collection tube). The middle fluid is pumped in the outer capillary in the same direction as the inner fluid to create a co-flow.

At the same time, the outermost (continuous) fluid is pumped inside the outer tube in the opposite direction to hydrodynamically focus the co-flow. When all fluids enter the collection tube, a double emulsion is formed, consisting of an inner fluid droplet within a larger middle fluid droplet, contained in the continuous fluid (Utada et al., 2007).

To fabricate the microfluidic device described by Utada et al. [134], the round glass capillaries with an inside diameter (I.D.) and outside diameter (O.D.) of 0.75 and 1.0 mm (World Precision Instruments, USA), were pulled in a Flaming/Brown micropipette puller (P-1000, Sutter Instrument Co., Carl Zeiss Canada Ltd, Toronto, Canada) to produce the tapered tips for injection and collection capillaries. The tips were then polished to the desired orifice size using a 7000 Grit abrasive paper as shown in Fig. 4. The tip size of the injection and collection glass tubes

Fig. 12. Collected microcapsules (contain liquid desiccant: 60 wt% LiBr and 40 wt% deionized water).

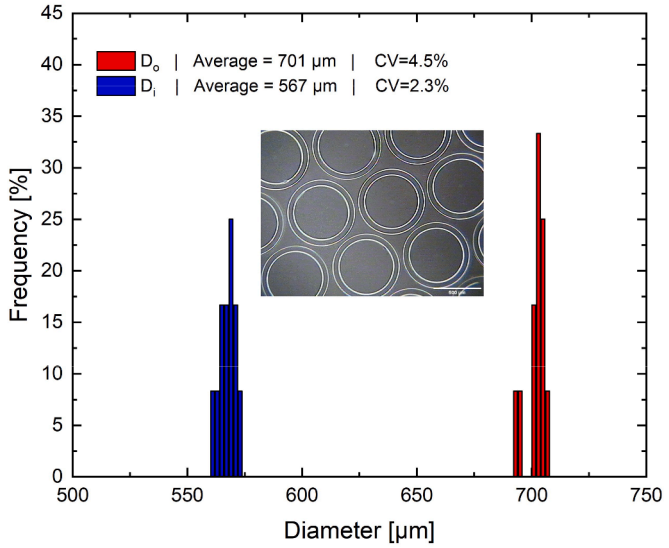

Fig. 13. The outer and inner diameter size distribution of microcapsules.

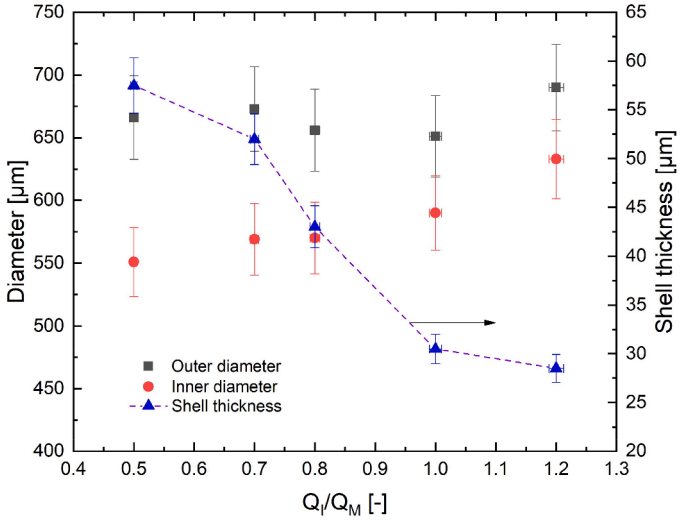

Fig. 15. The effect of flow rate ratios on inner diameter, outer diameter, and shell thickness.

were 40 and 300 μm, respectively. The tip of injection tube was treated with *n*- Octadecyltrimethoxysilane (OTMS) (Gelest Inc., USA) to make its surface hydrophobic, while the collection tube tip was treated with 3-[*methoxy*(*polyethyleneoxy*)6–9]propyltrimethoxysilane, tech-90 (Gelest Inc., USA) to render its surface hydrophilic. The chemical treatment was conducted by soaking the capillaries in the appropriate chemical for 60 min then dried in an oven temperature of 120 °C for 1–2 h. A glass round capillary tube with an I.D. and an O.D. of 1.12 and 1.5 mm (Gelest Inc., USA) was used to house the inner injection and collection tubes.

For the glass capillary device to function properly, perfect alignment of the injection and collection tube is required. For this purpose, Martino et al. (Martino et al., 2014) presented a 3D printed assembly to mount glass capillaries to ensure a perfect alignment. The assembly relied on the fabrication of screws that hold the inner (injection and collection) glass tubes. A set of two nuts were glided onto a slider and were used to mount the outer tube. The screws (holding the injection and collection tubes) were gently guided through the nut. Following the approach presented by Martino et al. (Martino et al., 2014), similar parts were designed and a 3D drawing for the assembly was prepared with the aid of SolidWorks software (Dassault Systèmes). The 3D drawings of the designed parts before and after the assembly are presented in Fig. 5, respectively. The parts were printed using an Objet30 PolyJet 3D printer (Stratasys, Ltd.). The 3D printed microfluidic device after the assembly is shown in Fig. 6a. The perfect alignment was confirmed by the images taken with a digital microscope (Unitron MEC2, Miller Microscopes) as shown by Fig. 6b.

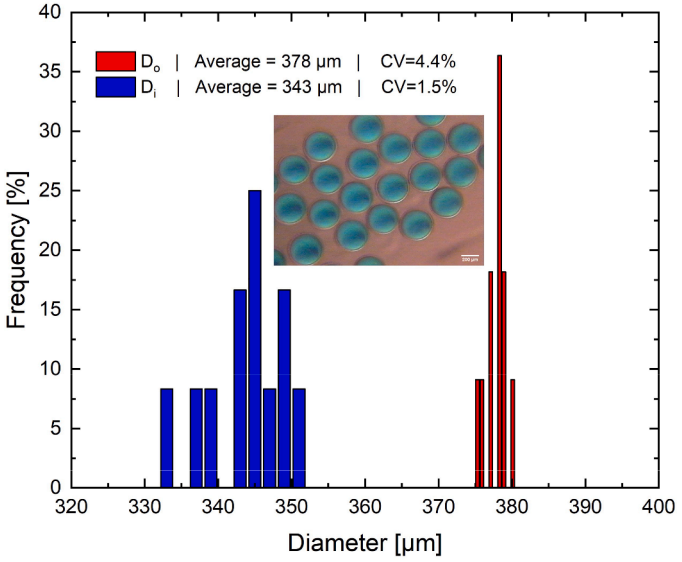

Fig. 16. The outer and inner diameter size distribution of microcapsules.

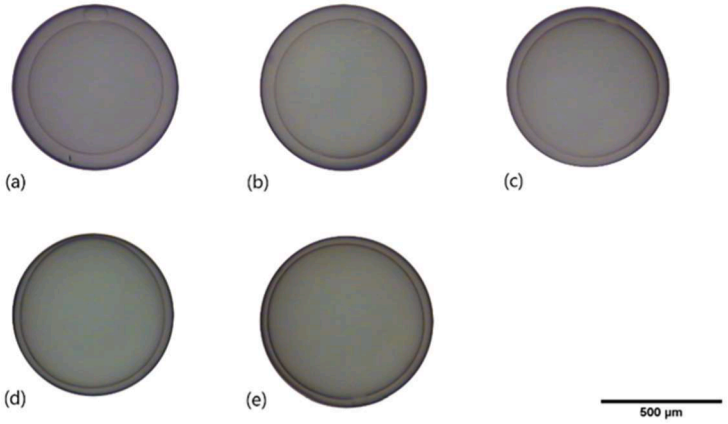

Fig. 14. The size of microcapsules with a LiBr 60 wt% at different Q_I/Q_M ratios: (a) 0.5; (b) 0.7; (c) 0.8; (d) 1.0; and (f) 1.2.

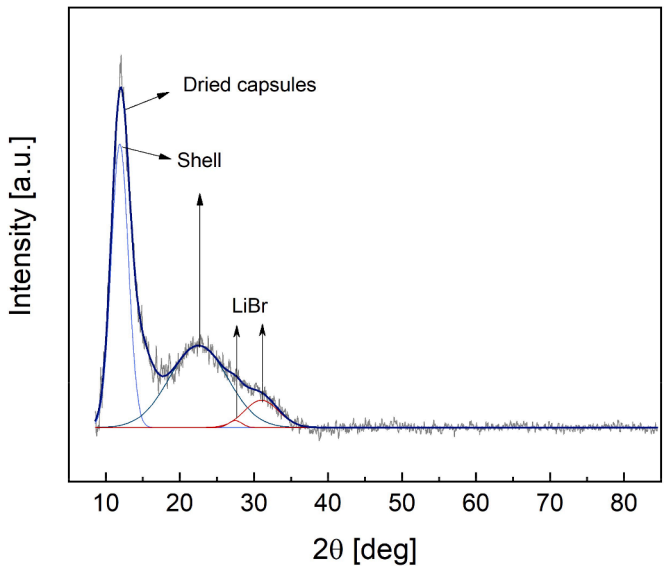

Fig. 17. X-ray diffraction patterns of the dried microcapsules (containing the LiBr salt), shell material, and pure LiBr salt.

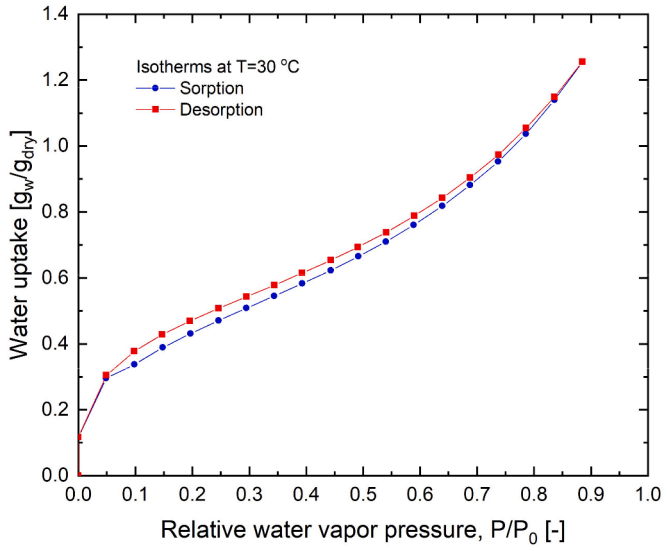

Fig. 18. The isotherm curve of the LiBr microcapsules.

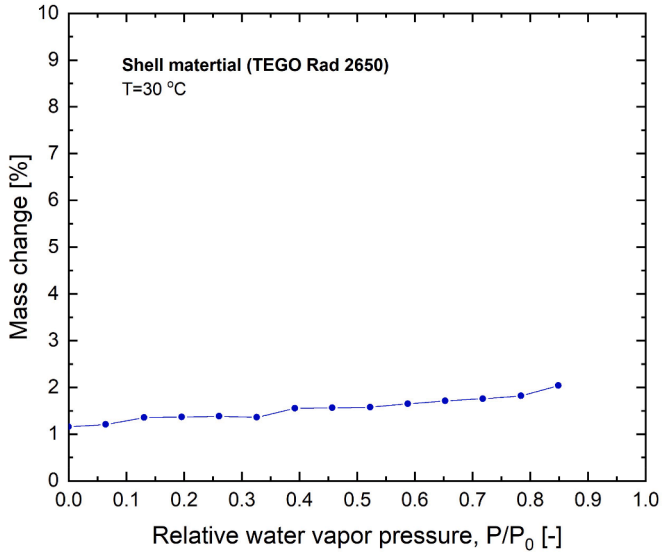

Fig. 19. The mass change of the shell material as a function of relative humidity.

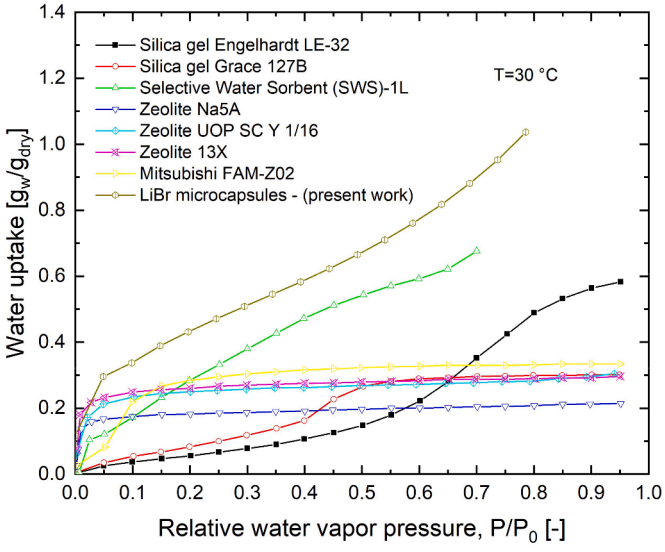

Fig. 20. The sorption capacity of capsules compared to common sorbent materials (Bales et al., 2005).

2.2. Microfluidic experimental setup

The inner fluid used in the experiments was an aqueous salt solution prepared by mixing a 60 wt% LiBr anhydrous salt (Sigma-Aldrich, Canada) and 40 wt% deionized water. Coloring dyes were added to the inner fluid mixture for better visualization. The middle phase was a mixture of 98 wt% TEGO Rad 2650 (donated by Evonik Industries, USA) and 2 wt% Irgacure 1173 Darocur photoinitiator (Sigma-Aldrich, Canada). The outer phase was a mixture composed of 59 wt% deionized water, 40 wt% glycerol, and a 1 wt% Pluronic F-127 surfactant (Sigma-Aldrich, Canada).

A schematic of the microfluidic experimental setup is shown in Fig. 7. The microfluidic device was mounted on the slide of a digital microscope (Unitron MEC2, Miller Microscopes) equipped with a microscope camera to observe the double emulsion formation. One syringe pump (Model 11 Plus, Harvard Apparatus) was used to inject the inner fluid to the inlet of the microfluidic device at a rate of 5–10 mL/h. Another two syringe pumps (NE-300, New Era) were used to introduce the middle fluid and outer fluid at a rate of 5–10 mL/h and 50–60 mL/h, respectively. The microcapsules exited the microfluidic device via polyethylene tubing (BD Intramedic) with an I.D. and O.D. of 1.19 and 1.70 mm, respectively. A commercial UV-LED with a 365 nm wavelength, 50 W power, and a 235 mW/cm^2 intensity was used for the in-line curing of the freshly produced microcapsules. The encapsulated liquid sorbent with the cured shell was collected in a vial. The microfluidic setup used to conduct the experiment is shown in Fig. 8. The collected microcapsules were washed in deionized water multiple times to remove any carrier fluid residues, and they were finally stored in a glass vial. ImageJ software was used to analyze the circularity and measure the sizes of 50 microcapsules.

2.3. Characterization of microcapsules

To confirm that the observed crystalline structure in the microscopic images of the microcapsules is indeed a LiBr salt, a small batch of microcapsules was packed into a quartz capillary. The bead-filled capillary

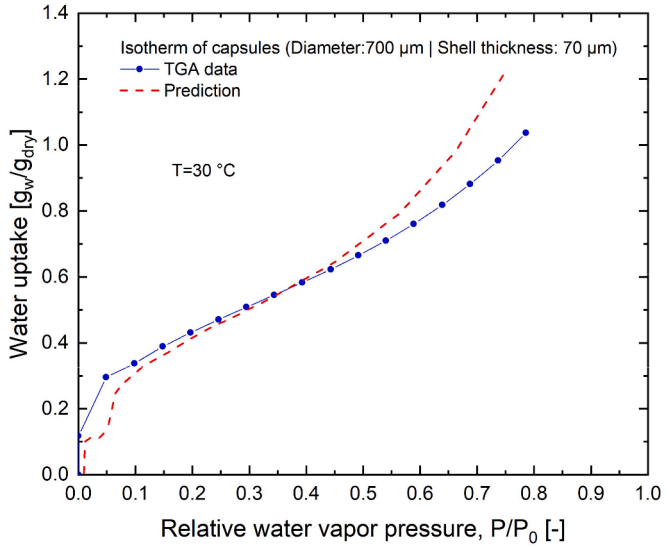

Fig. 21. The isotherm curve of the microcapsules: (a) the thermogravimetric analyzer (TGA) data; and (b) the prediction.

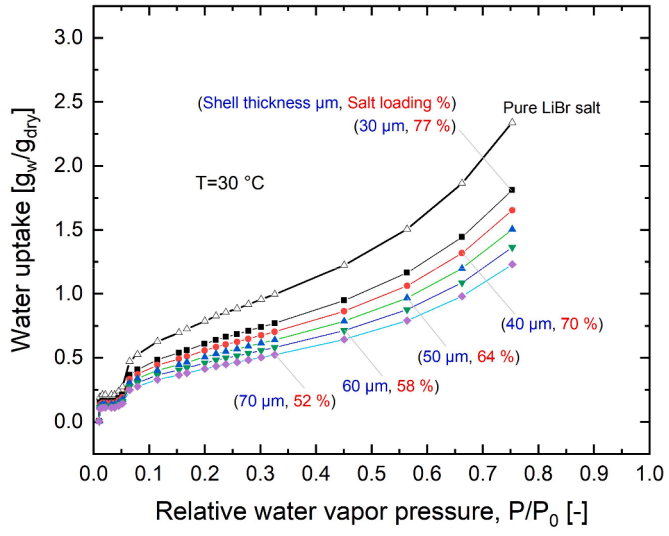

Fig. 22. The predicted isotherm curves of the microcapsules of various sizes.

was then placed in a vacuum oven at 48 °C for 1.5 days, after which clay was used to seal the open end, and the X-diffraction pattern was acquired immediately by using a D8 ADVANCE, Bruker diffractometer at 4D LABS, SFU. X-ray patterns were also acquired for the pure LiBr salt and the cured shell material sample as references.

Water sorption isotherms (water vapor pressure: 0–2.1 kPa, corresponding to the relative humidity (RH) of 0–70% for a ~18 mg sample that contained capsules (a 60 wt% LiBr solution) were measured using a thermogravimetric vapor sorption analyzer (IGA-002, Hiden Isochema). The temperature of the chamber that contained the sample was fixed at 30 °C. The pressure was increased with 2 mbar (20 kPa) steps, and in every step, the sample was given enough time to reach equilibrium. To measure dry weight, the sample was dried under vacuum for 6 h at 80 °C at the end of the test.

To reveal the morphology of the shell material of microcapsule, scanning electron microscope (SEM) images were acquired using the microscope facility (Nova NanoSEM, FEI) at 4D LABS, SFU.

2.4. Multi-cycle performance test

To investigate the long-term sorption performance of the produced microcapsules, a small batch of microcapsules that contain the LiBr liquid desiccant was selected for an accelerated muti-cycle performance testing using thermogravimetric vapor sorption analyzer (IGA-002, Hiden Isochema). Pressure swing sorption-desorption cycles were performed between 0 and 2.1 kPa at 30 °C.

2.5. Mechanical testing

2.5.1. Compression test

To examine the mechanical integrity of the capsules, compression and expansion tests were performed. The compression test was performed using a thermomechanical analyzer (TMA) (Q400EM, TA instruments, see Fig. 9). The capsules were placed on the stage of the instrument, and a standard expansion probe with a 6.07 mm diameter contact area was used to apply a force of 0.05 N per minute ramp rate as shown in Fig. 10. The tests were conducted in a dry nitrogen environment at 20 °C.

2.5.2. Expansion test

The elastic capsules will be subjected to cyclic expansion pressure when they go through the absorption/desorption process. Therefore, a sample of the capsules was immersed in a water bath for 3 h to promote the osmotic swelling due to the presence of the salt inside the capsules. A control sample which was used as a reference was soaked in a LiBr salt solution with the same concentration as that of the inner core (60 wt% LiBr) to reach osmotic equilibrium.

3. Results and discussion

3.1. Microcapsule design and fabrication

The actual production of the microcapsules in the microfluidic device (before UV curing) is shown in Fig. 11. The collected microcapsules (after washed in deionized water multiple times) are shown in Fig. 12. The average outer and inner (core) diameters of the capsules were 700 and 570 μm, respectively, as presented in Fig. 13. The average measured mass of the capsules was 0.5 mg; heavy enough to not be carried over by the air stream during the dehumidification process. The coefficient of variation (CV) for the outer and the inner diameter is 4.4% and 1.5%, respectively, which means the capsules are monodisperse (CV<5%).

To demonstrate that the size of the capsules can be adjusted by the changing the flow rates of the fluids, the mass flow rate of middle (Q_M) and outer fluids (Q_o) were fixed at 6.0 and 50 mL/h, respectively, while the flow rate of the middle fluid (Q_I) was varied between 3 and 7 mL/h. The produced capsules at the various ranges of Q_I/Q_M ratios are shown in Fig. 14. The variation of shell thickness, inner and outer diameters of the capsules as a function of the Q_I/Q_M ratio is shown in Fig. 15. It can be observed from Fig. 15 that the ratio has a little effect on the outer diameter, while the inner diameter increases by increasing the Q_I/Q_M ratio. It can be concluded that the shell thickness can be decreased by increasing the Q_I/Q_M ratio.

The outer diameter of the microcapsules can also be adjusted by adjusting the outer (carrier) fluid flow rates. A batch with smaller microcapsules was produced by increasing the outer fluid flow rate. The average outer and inner (core) diameters of the capsules were 378 and 343 μm, respectively, as presented in Fig. 16.

3.2. Characterization of the microcapsules

The X-ray patterns for the bulk LiBr salt, shell material, and the dried microcapsules are shown in Fig. 17. To analyze the results, the peaks in the X-ray pattern of the dried microcapsules were deconvoluted and compared with the reference patterns of the shell material and the pure

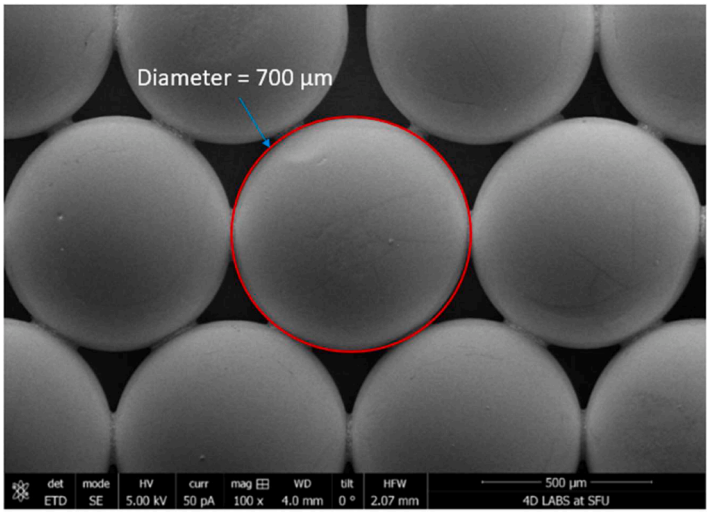

Fig. 23. A scanning electron microscope image of the shell's outer surface.

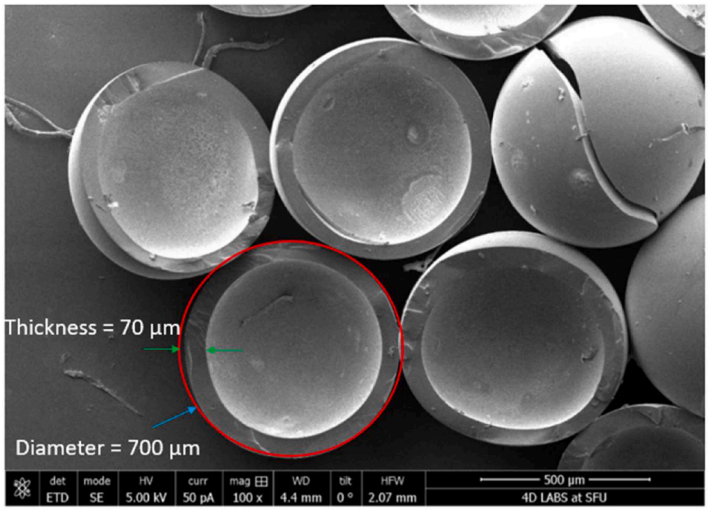

Fig. 24. A scanning electron microscope image of a shell's cross-section.

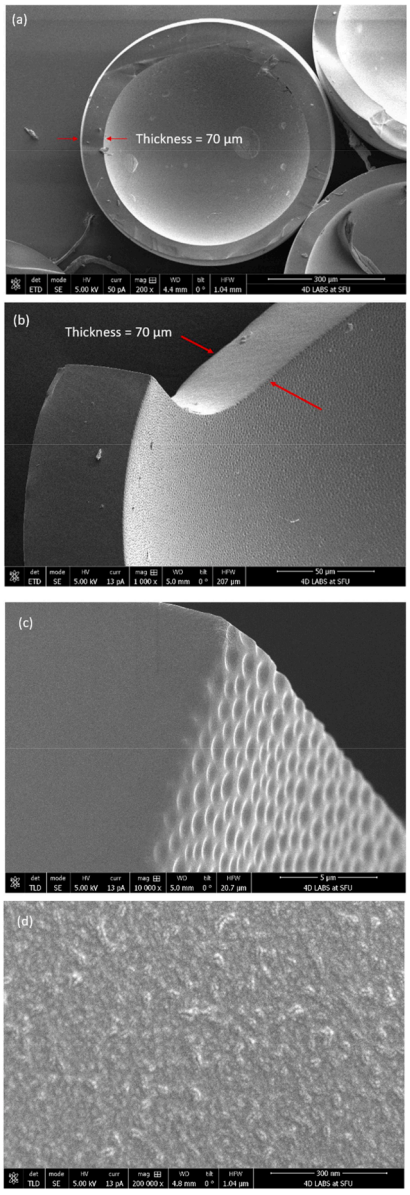

Fig. 25. High magnification (a) 200x; (b)1000x; (c)10,000x, and (d) 200,000x scanning electron microscope images of the shell cross-section.

LiBr salt. The peaks that centered at ~12 and 22° are related to the shell material, and the peaks at ~27.5 and 31° are assigned to the LiBr salt. The relative reduction of the LiBr peak intensities relates to the coverage of shell material that affects the X-ray peak intensities and also peak positions.

The collected isotherms curves, from the thermogravimetric vapor sorption analyzer test, for the absorption and desorption processes are shown in Fig. 18. The data indicated that there is not a considerable hysteresis or any salt/solution leakage as the absorption and desorption curves were almost identical. The linear water uptake in 10–70% RH indicates that the vapor is absorbed (or desorbed) by the sorbent in its liquid phase. The sharp drop in water uptake below 10% RH indicates the formation of solid hydrates (crystals).

As the shell is made of a membrane, a thermogravimetric test was also performed for the (cured) shell sample to investigate its impact on the final sorption capacity of the microcapsules. The results, presented in Fig. 19, revealed that change in relative water vapor pressure does not result in any significant change in the mass of the shell material.

The comparison between the sorption capacity of the capsules and the common solid sorbent material in the literature shows that the capsules have a higher capacity, as presented in Fig. 20.

By having identical microcapsules of the same size, the isotherm curves can be predicted at any given size given the outer diameter, shell thickness, and reference isotherm curve of the pure salt. Fig. 21 shows that the predicted isotherm curve is in good agreement with experimental data collected by the thermogravimetric vapor sorption analyzer for the produced LiBr microcapsules (outer diameter =700 µm, and shell thickness =70 µm). Fig. 22 shows the predicted isotherm curves for 700 µm microcapsules with various shell thicknesses. From the graph, the actual salt loading (i.e., the ratio of the salt mass to the total dry weight of the microcapsules) can be estimated, and it was found that for the prepared microcapsules, the estimated salt loading is 54%.

An SEM image for the outer surface of microcapsules is shown in Fig. 23. The average size of the capsules is approximately ~700 µm. The shell that contains the liquid sorbent was perfectly spherical and no salt was observed on the outer surface of the shell which indicated that the shell was able to contain the salt and its solution without leakage issues.

The SEM image for the cross-section of the shell after few microcapsules were cut into halves using a sharp razor blade is presented in Fig. 24. The average shell thickness of the capsules was around ~70 µm. The inner surface of the shell looks very smooth and free of any imperfections as shown in Fig. 25a. Scanning electron microscope images with high magnification (Fig. 25b and Fig. 25c) showed that there were dimples that were small in size (few nanometers) on the surface of the shell. A higher magnification image (Fig. 25d) confirmed that the shell was made of a dense membrane, and that probably there would not be any leakages (salt particles or liquid solution) from the capsules.

3.3. Capsule morphology during dehydration and rehydration

The morphology of the capsules during dehydration and rehydration is presented by the microscopic images in Fig. 26. A capsule was heated in the oven at 90 °C for 3 h to dehydrate the capsule (partially remove the water). Due to the elasticity of the shell, the capsule buckled as shown in Fig. 26a. The capsule then rehydrated by leaving the capsule in the room environment (~20 °C and ~50% RH) for 3 h. Interestingly, the capsule was able to regain its shape and the salt hydrates (formed during the dehydration) were detected as shown in Fig. 26b. This confirms that capsules can tolerate salt crystallization which is beneficial for increasing the sorption capacity. The capsule was then placed inside a water bath for 3 h to completely hydrate it and dissolve the salt hydrates as shown in Fig. 26c.

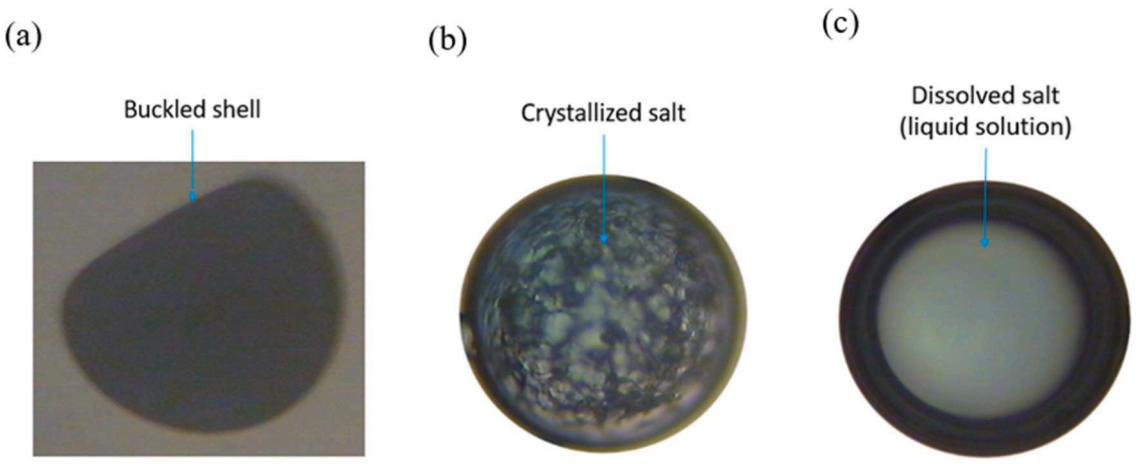

Fig. 26. (a) A collapsed shell after dehydration (desorption); (b) a collapsed shell after partial rehydration (absorption); and (c) complete rehydration in a water bath.

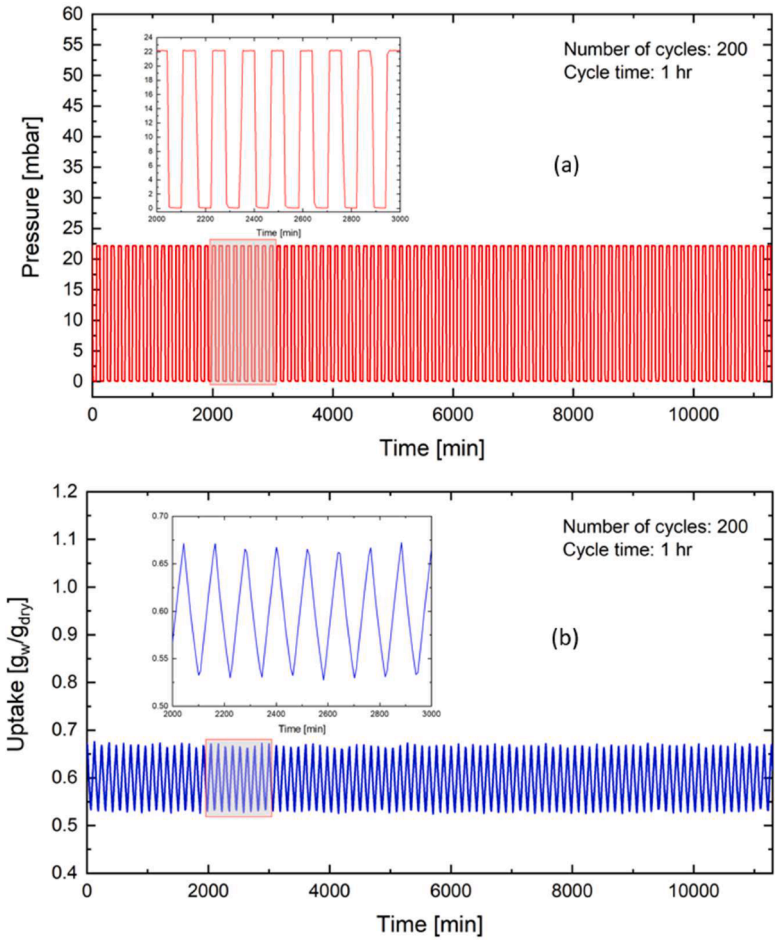

Fig. 27. (a) LiBr microcapsules (at 30 °C) uptake change; and (b) pressure swing (0–2.1 kPa) during sorption-desorption cycles.

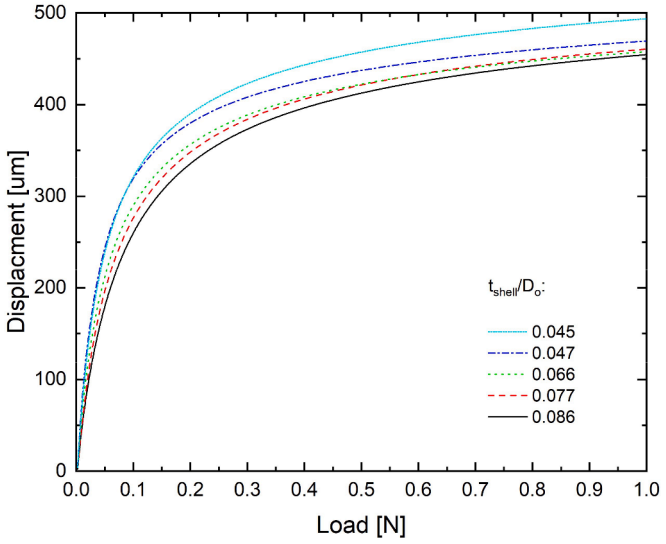

Fig. 28. Compression testing: displacement as a function of applied load.

3.4. Multi-cycle performance test

The data collected from the thermogravimetric vapor sorption analyzer during the rapid pressure swing sorption-desorption cycles is shown in Fig. 27. It was found that the uptake capacity of the capsules did not change even after 200 cycles as presented in Fig. 27b and the capsules remained intact.

3.5. Mechanical testing

The result from the thermomechanical analyzer during the compression test is shown in Fig. 28. The measured displacement as a function of applied load for capsules with various shell thicknesses to the outer diameter ratio (t_{shell}/D_o). The results show that capsules can withstand up to a 1 Newton force (about 100 *g* mass) without breaking. This suggests that a capsule can withstand a force of up to 2×10^5 its weight (~0.5 mg). It is worth noting that by repeating the test multiple times, some capsules with a t_{shell}/D_o=0.045 ruptured. This is due to their thin shell. Therefore, it is recommended that the capsules be fabricated with a ratio of t_{shell}/D_o=0.047 or higher to ensure the mechanical integrity with acceptable shell mass transfer resistance.

Microscopic images of samples in a LiBr solution and a water bath during the expansion test are shown in Fig. 29. By comparing the measured shell thickness in both samples, it appears that, due to the osmotic swelling, the outer diameter of the capsules increased by 6% and the shell became ~28% thinner without affecting the integrity of the capsules.

4. Conclusion

Spherical micro-absorbers that can be used for dehumidification systems were produced using a microfluidic technique to encapsulate the liquid LiBr desiccant inside a semi-permeable polymeric membrane shell. Due to the indirect contact between the liquid desiccant and the air in this design, problems such as solution carryover and corrosion that are associated with the conventional packed-column absorbers can be completely eliminated. The formed spherical micro-absorbers (i.e., microcapsules) were highly uniform in size and can be designed to have a micro-scale size (500–1000 μm diameter) with an adjustable shell thickness. They provide high reaction surface-to-volume ratios (6000–12,000 m^2/m^3) that allows fast absorption rates, therefore, more compact absorber designs. To achieve the required dehumidification effect, thousands of microcapsules should be produced and used in a single setup to create enough moisture removal capacity. This can be achieved by simply packing the microcapsules in a packed-bed configuration, or coating the capsules on substrates to avoid the high pressure drops associated with packed-beds.

The recommendations for future work are as follows:

- Attempt the encapsulation of other liquid desiccants, such as $CaCl_2$ and LiCl and evaluating the sorption capacity of the produced microcapsules.
- Investigate the possibility of increasing the salt loading inside the microcapsules to increase the sorption capacity.
- Investigate scale-up methods to produce microcapsules at an industrial level.
- Investigate the heat/mass performance of the micro-absorbers with the various liquid desiccants for dehumidification applications.
- Design and build an optimized pilot-scale absorber, and perform tests under real-life testing conditions.

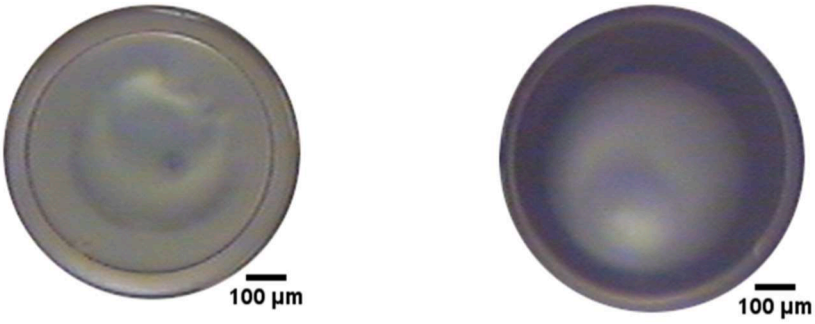

Fig. 29. The size of the microcapsule with 60 wt% LiBr (sol.) soaked in: (a) 60 wt% LiBr solution (D_o=686 μm, D_i=577 μm); and (b) deionized water (D_o=726 μm, D_i=648 μm).

Declaration of Competing Interest

The authors declare that they have no known competing financial interests or personal relationships that could have appeared to influence the work reported in this paper.

Acknowledgement

The authors gratefully acknowledge the financial support of the Natural Sciences and Engineering Research Council of Canada (NSERC) through the Advancing Climate Change Science in Canada Grant No. ACCPJ 536076-18, and NSERC Discovery Grant No. RGPIN-2022-04371.

References

Ali, A.H.H., Schwerdt, P., 2009. Characteristics of the membrane utilized in a compact absorber for lithium bromide–water absorption chillers. Int. J. Refrig. 32, 1886–1896.

Bales, C., Gantenbein, P., Hauer, A., Henning, H.-M., Jaenig, D., Kerskes, H., et al., 2005. Thermal properties of materials for thermo-chemical storage of solar heat. Rep B2-IEA SHC Task 32.

Bassuoni, M.M., 2011. An experimental study of structured packing dehumidifier/regenerator operating with liquid desiccant. Energy 36, 2628–2638.

Bhowmik, M., Muthukumar, P., Anandalakshmi, R., 2021. Experimental investigation on structured packed bed liquid desiccant dehumidifier: an optimal mixture design of experiments strategy. Int. J. Refrig. 122, 232–244.

Chen, T., Dai, Z., Yin, Y., Zhang, X., 2017. Experimental investigation on the mass transfer performance of a novel packing used for liquid desiccant systems. Sci Technol Built Environ 23, 46–59.

Chugh, D., Gluesenkamp, K., Abdelaziz, O., Moghaddam, S., 2017. Ionic liquid-based hybrid absorption cycle for water heating, dehumidification, and cooling. Appl. Energy 202, 746–754.

Dong, H.-W., Cho, H.-J., Park, J.-Y., Jeong, J.-W., 2019. Optimum regeneration temperature of a desiccant solution in a packaged liquid desiccant-assisted air conditioning unit. Int. J. Refrig. 101, 155–166.

Elsarrag, E., M Ali, E.E., Jain, S, 2005. Design guidelines and performance study on a structured packed liquid desiccant air-conditioning system. HVAC\&R Res 11, 319–337.

Farooq, M., Wahid, A., Kobayashi, N., Fujita, D., Basra, S.M.A., 2009. Plant drought stress: effects, mechanisms and management. Sustain. Agric., Springer 153–188.

Fernández-Seara, J., Diz, R., Uh\'\ia, F.J., Dopazo, A., Ferro, J.M, 2011. Experimental analysis of an air-to-air heat recovery unit for balanced ventilation systems in residential buildings. Energy Convers. Manag. 52, 635–640.

Guieysse, B., Hort, C., Platel, V., Munoz, R., Ondarts, M., Revah, S., 2008. Biological treatment of indoor air for VOC removal: potential and challenges. Biotechnol. Adv. 26, 398–410.

Han, J., Guo, H., Brad, R., Gao, Z., Waterer, D., 2015. Dehumidification Requirement for aGreenhouse Located in a Cold Region. Appl. Eng. Agric. 31, 291–300.

Jain, S., Bansal, P.K., 2007. Performance analysis of liquid desiccant dehumidification systems. Int. J. Refrig. 30, 861–872.

Liao, X., Radermacher, R., 2007. Absorption chiller crystallization control strategies for integrated cooling heating and power systems. Int. J. Refrig. 30, 904–911.

Liu, X.H., Yi, X.Q., Jiang, Y., 2011. Mass transfer performance comparison of two commonly used liquid desiccants: LiBr and LiCl aqueous solutions. Energy Convers. Manag. 52, 180–190.

Longo, G.A., Gasparella, A., 2006. Experimental analysis on chemical dehumidification of air in a packed column by hygroscopic salt solution: comparison between structured and random packings. HVAC&R Res 12, 713–729.

Martino, C., Berger, S., Wootton, R.C.R., deMello, A.J, 2014. A 3D-printed microcapillary assembly for facile double emulsion generation. Lab Chip 14, 4178–4182.

Mei V.C., Chen F.C., Lavan Z., Collier Jr. R.K., Meckler G. An assessment of desiccant cooling and dehumidification technology. 1992.

Nizovtsev, M.I., Borodulin, V.Y., Letushko, V.N., Zakharov, A.A., 2016. Analysis of the efficiency of air-to-air heat exchanger with a periodic change in the flow direction. Appl. Therm. Eng. 93, 113–121.

Qi, R., Dong, C., Zhang, L-Z., 2020. A review of liquid desiccant air dehumidification: from system to material manipulations. Energy Build. 215, 109897.

Rafique, M.M., Gandhidasan, P., Bahaidarah, H.M.S., 2016. Liquid desiccant materials and dehumidifiers–A review. Renew Sustain. Energy Rev. 56, 179–195.

Singh, R.P., Mishra, V.K., Das, R.K., 2018. Desiccant materials for air conditioning applications-A review. IOP Conf. Ser. Mater. Sci. Eng. 404, 12005.

Tan, L.S., Shariff, A.M., Lau, K.K., Bustam, M.A., 2012. Factors affecting CO2 absorption efficiency in packed column: a review. J. Ind. Eng. Chem. 18, 1874–1883.

Utada, A.S., Chu, L-Y, Fernandez-Nieves, A., Link, D.R., Holtze, C., Weitz, D.A., 2007. Dripping, jetting, drops, and wetting: the magic of microfluidics. MRS Bull. 32, 702–708.

Utada, A.S., Lorenceau, E., Link, D.R., Kaplan, P.D., Stone, H.A., Weitz, D.A., 2005. Monodisperse double emulsions generated from a microcapillary device. Science (80-) 308, 537–541.

Vericella, J.J., Baker, S.E., Stolaroff, J.K., Duoss, E.B., Hardin, J.O., Lewicki, J., et al., 2015. Encapsulated liquid sorbents for carbon dioxide capture. Nat. Commun. 6, 1–7.

Wang, K., Abdelaziz, O., Kisari, P., Vineyard, E.A., 2011. State-of-the-art review on crystallization control technologies for water/LiBr absorption heat pumps. Int. J. Refrig. 34, 1325–1337.